Monthly Notices
of the
ROYAL ASTRONOMICAL SOCIETY

MNRAS **461,** 4115–4124 (2016)
Advance Access publication 2016 July 7

doi:10.1093/mnras/stw1585

The CHARA Array resolves the long-period Wolf–Rayet binaries WR 137 and WR 138

Noel D. Richardson,[1]★ Tomer Shenar,[2] Olivier Roy-Loubier,[3] Gail Schaefer,[4] Anthony F. J. Moffat,[3] Nicole St-Louis,[3] Douglas R. Gies,[5] Chris Farrington,[4] Grant M. Hill,[6] Peredur M. Williams,[7] Kathryn Gordon,[5] Herbert Pablo[3] and Tahina Ramiaramanantsoa[3]

[1]*Ritter Observatory, Department of Physics and Astronomy, The University of Toledo, Toledo, OH 43606-3390, USA*
[2]*Institut für Physik und Astronomie, Universität Potsdam, Karl-Liebknecht-Str. 24/25, D-14476 Potsdam, Germany*
[3]*Département de physique and Centre de Recherche en Astrophysique du Québec (CRAQ), Université de Montréal, C.P. 6128, Succ. Centre-Ville, Montréal, Québec, H3C 3J7, Canada*
[4]*The CHARA Array, Mount Wilson Observatory, 91023 Mount Wilson, CA 91023, USA*
[5]*Center for High Angular Resolution Astronomy, Department of Physics and Astronomy, Georgia State University, PO Box 5060, Atlanta, GA 30302-5060, USA*
[6]*W. M. Keck Observatory, 65-1120 Mamalahoa Highway, Kamuela, HI 96743, USA*
[7]*Institute for Astronomy, University of Edinburgh, Royal Observatory, Edinburgh EH9 3HJ, UK*

Accepted 2016 June 30. Received 2016 June 30; in original form 2016 April 1

ABSTRACT

We report on interferometric observations with the CHARA Array of two classical Wolf–Rayet (WR) stars in suspected binary systems, namely WR 137 and WR 138. In both cases, we resolve the component stars to be separated by a few milliarcseconds. The data were collected in the *H* band, and provide a measure of the fractional flux for both stars in each system. We find that the WR star is the dominant *H*-band light source in both systems ($f_{\rm WR,137} = 0.59 \pm 0.04$; $f_{\rm WR,138} = 0.67 \pm 0.01$), which is confirmed through both comparisons with estimated fundamental parameters for WR stars and O dwarfs, as well as through spectral modelling of each system. Our spectral modelling also provides fundamental parameters for the stars and winds in these systems. The results on WR 138 provide evidence that it is a binary system which may have gone through a previous mass-transfer episode to create the WR star. The separation and position of the stars in the WR 137 system together with previous results from the IOTA interferometer provides evidence that the binary is seen nearly edge-on. The possible edge-on orbit of WR 137 aligns well with the dust production site imaged by the *Hubble Space Telescope* during a previous periastron passage, showing that the dust production may be concentrated in the orbital plane.

Key words: binaries: visual – stars: individual: WR 137 – stars: individual: WR 138 – stars: mass-loss – stars: winds, outflows – stars: Wolf–Rayet.

1 INTRODUCTION

Every star is described with a set of fundamental parameters including its radius, *R*, mass, *M*, luminosity, *L*, and effective temperature, $T_{\rm eff}$. For most stars, we must estimate these from accurate photometry, a measure of the distance, and a reliable spectrum. This can be calibrated using techniques involving binary stars where we either utilize an eclipsing system to understand fundamental parameters or where a visually resolved orbit can allow us to infer the stellar masses of the binary. Recent progress has been made in the area of fundamental parameters through interferometric techniques (e.g. Boyajian et al. 2012) where long-baseline interferometry can resolve single stars, yielding direct measures of angular diameters. When coupled with a spectral energy distribution (SED) and distance, measurements of stellar radii and temperatures are possible to accuracies of a few per cent allowing accurate predictions for other stars (Boyajian, van Belle & von Braun 2014).

Empirical relations for massive stars are more complicated to determine due to their scarcity and large distances. Even with a large binary fraction (e.g. Sana et al. 2014; Aldoretta et al. 2015), the calibration of stellar parameters has relied on eclipsing binaries.

★E-mail: noel.richardson@UToledo.edu

Sana et al. (2012) show that most massive stars with periods of $P \lesssim 1000$ d will either interact in the future or have already interacted. Therefore, most stars that are used to calibrate the mass–radius–luminosity relationships for massive stars (Martins, Schaerer & Hillier 2005) are not representative of single-star evolution. If we wish to understand the evolution of massive stars without binary effects, we need to measure directly masses for evolved stars in long-period, widely separated binaries. In order to measure the masses of these stars, as well as place lower limits on the mass-loss of the more evolved component, we must visually resolve the orbits of nearby systems where we can also obtain a double-lined spectroscopic orbit.

The Wolf–Rayet (WR) stars represent a class of objects with great potential to determine the empirical lower limits to the mass lost by massive stars, which Smith & Owocki (2006) speculate could be up to 65 per cent of the mass of a 60 $M_\odot$ star prior to the supernova explosion. Thus far, only two WR systems have been examined with interferometry. They are γ^2 Velorum (Hanbury Brown et al. 1970; Millour et al. 2007; North et al. 2007) and WR 140 (Monnier et al. 2004, 2011). Both systems have well-defined double-lined spectroscopic orbits (Schmutz et al. 1997; Fahed et al. 2011) and consist of a carbon-rich WC star orbiting an O star. For γ^2 Vel, the spectral types of the component stars are WC8+O7.5III (Schmutz et al. 1997), while for WR 140, they are WC7pd+O5.5fc (Fahed et al. 2011).

The first results on γ^2 Vel (WR 11, HD 68273) were presented by Hanbury Brown et al. (1970), who found that the Narrabri Intensity Interferometer could be used not only to resolve single hot stars as it was designed for, but also to resolve binary orbits and determine the angular sizes of the emission line forming regions for some hot stars. As such, they derived a separation of the binary ($P = 78.5$ d) of 4.3 ± 0.5 mas, corresponding to a distance of 350 ± 50 pc when compared to the double-lined spectroscopic orbit. Further, Hanbury Brown et al. found that the emission line region was $0.24a$ in relation to the semi-major axis, a. γ^2 Vel was then studied with VLTI/AMBER in the near-infrared (NIR) by Millour et al. (2007). These results proved that the expected visual orbit was fairly well constrained at the time of the observation, and that the predicted WR and O star fluxes were compatible with the previous modelling of the system (De Marco & Schmutz 1999; De Marco et al. 2000). Further, they found that roughly 5 per cent of the flux in the K band was from the free–free emission in the wind–wind collision region. Finally, North et al. (2007) observed γ^2 Vel across its entire orbit with the Sydney University Stellar Interferometer to obtain a visual orbit and measure the distance to an unprecedented precision of 336^{+8}_{-7} pc. The resulting masses were $M_{\rm WR} = 9.0 \pm 0.6\,M_\odot$ and $M_{\rm O} = 28.5 \pm 1.1\,M_\odot$, and represent the best measured mass for any WR star.

WR 140 (HD 193793) is a prototype for colliding wind systems with a highly elliptical ($e = 0.896$), long-period ($P = 7.93$ yr) orbit. The system was resolved with the IOTA3 Imaging Interferometer by Monnier et al. (2004), and then Monnier et al. (2011) combined the IOTA3 measurements and new CHARA measurements with the radial velocity (RV) orbit based on an intensive spectroscopic campaign by Fahed et al. (2011) to measure the visual orbit precisely and then derive the masses of the component stars to be $M_{\rm WR} = 14.9 \pm 0.5\,M_\odot$ and $M_{\rm O} = 35.9 \pm 1.3\,M_\odot$, with the system at a distance of 1.67 ± 0.03 kpc.

Two long-period WR stars are obvious candidates for follow-up long-baseline interferometry: WR 137 and WR 138. WR 137 (HD 192764) consists of a WC7pd + O9 binary with a period of 13.05 yr and a small eccentricity of $e = 0.18$ (Lefèvre et al. 2005). It has a known RV orbit (at least for the WR component; the O star's orbit is very noisy) with $a \sin i = 15$ au, which combined with a distance of 1.82 kpc (Nugis & Lamers 2000) yields a value of ∼8 mas, well within the reach of modern interferometers. In fact, a preliminary interferometric result presented by Rajagopal (2010) indicates that the binary was resolved by the IOTA interferometer in the H band, with a flux ratio measured relative between the two stars of $f_2/f_1 = 0.81$ and a separation of 9.8 mas in 2005, although the flux ratio is ambiguous as to which component star is represented by which. This makes this system appealing to observe with follow-up observations so that a third WR+O system can be resolved. Further, the system is a known dust producer (Williams et al. 1985, 2001; Marchenko, Moffat & Grosdidier 1999), so multi-wavelength interferometric observations could reveal the location of dust formation in these particular colliding wind systems that form dust spirals (e.g. Tuthill et al. 2008).

WR 138 (HD 193077) is a potential long-period binary consisting of a WN5o (Smith, Shara & Moffat 1996) and an O9 star (Annuk 1990), although the classification of the secondary has not been well constrained. Annuk (1990) presented the orbital elements for the WR and O components. The putative orbit has a period of $P = 4.21$ yr (1538 d) and $e = 0.3$. The period was confirmed to be 1521 ± 35 d with additional data presented by Palate et al. (2013), although their newer data were too sparse to better fit the orbital elements. Further, Palate et al. (2013) found that the X-ray emission was fully consistent with a colliding wind binary. The WR RV curve is much better defined than that of the O star, which shows an apparent, low-amplitude, variation in anti-phase to the WR star. With a measurement of $a \sin i = 4.3$ au, we expect a separation of ∼2.2 mas when combined with an estimated distance of 1.9 kpc (from the mean of that for WR 133 and WR 139 in the same association[1]). However, the O-component absorption lines of WR 138 are very broad and shallow, leading Massey (1980) to claim that WR 138 was a single, newly formed WR star with intrinsic broad absorption lines. Interferometry can resolve the issue by either resolving two stars or showing an unresolved star. With very broad absorption lines, the secondary would more likely be a main-sequence star.

In this paper, we present interferometric observations of WR 137 and WR 138 with the CHARA Array that show that both of these systems are resolved with long-baseline NIR interferometry. Section 2 outlines our interferometric observations. In Section 3, we show the binary fits for the observations. We discuss these systems in Section 4, and present goals of future studies and conclude this paper in Section 5.

2 LONG-BASELINE INTERFEROMETRY WITH THE CHARA ARRAY

We collected long-baseline NIR interferometry of WR 137 and WR 138 using the CHARA Array (ten Brummelaar et al. 2005) and CLIMB beam combiner (ten Brummelaar et al. 2013) in the H band during the nights of 2013 August 13–14. The CHARA Array is a Y-shaped interferometric array of six 1 m telescopes with baselines ranging from 34 to 331 m in length. Our observations used longer baselines consisting of the S1, E2, and W1 telescopes which yield maximum baselines between 251 and 278 m. The observations are summarized in Table 1.

[1] as listed in Rosslowe & Crowther (2015) at http://pacrowther.staff.shef.ac.uk/WRcat/

Table 1. CHARA interferometric observing log.

UT date	Baselines	Baseline length(s) (m)	N_{137}	N_{138}	Calibrator HD number(s)
2013 Aug. 14	S1/E2/W1	278, 251, 278	2	2	191703, 192804
2013 Aug. 15	S1/E2/W1	278, 251, 278	3	0	191703, 192804, 192536

Table 2. Calibrator stars.

HD number	Spectral type	Reference	Angular diameter (mas)	Nights used
191703	F0V	Honeycutt & McCuskey (1966)	0.21 ± 0.01	2013 Aug. 13, 14
192804	F8V	Ljunggren & Oja (1961)	0.23 ± 0.01	2013 Aug. 13, 14
192536	A7III	Barbier (1963)	0.17 ± 0.01	2013 Aug. 14

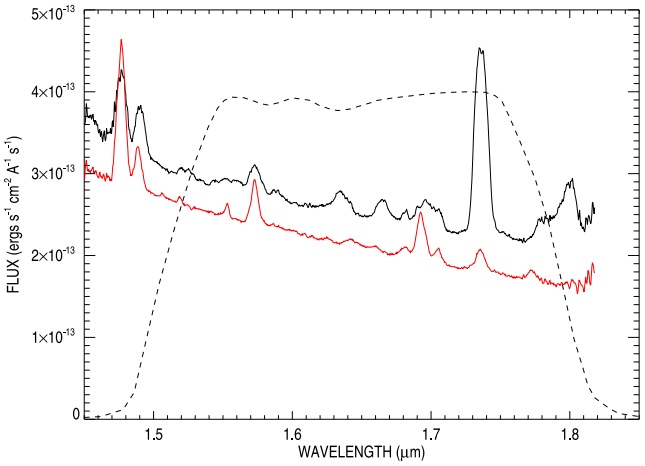

Figure 1. NIR spectra of WR 137 (black) and WR 138 (red) from Shara et al. (2012) are shown, with an *H*-band filter response function overplotted as a dashed line. For WR 137, the strong emission lines of C IV λ1.736 μm can drastically alter the instrumental response of the CHARA Array, and were accounted for through comparison of the Fourier spectrum of the fringe envelopes of the calibrator and target stars. In contrast, the weaker lines in the spectrum of WR 138 account for very little difference in the instrumental response.

To measure the instrument response and calibrate our data, we observed calibrator stars with small angular diameters both before and after each observation of a target star. Namely, we observed the calibrator stars listed in Table 2. In order to calibrate correctly our data, we fit these stars' SEDs with Kurucz model atmospheres corresponding to the spectral types previously published. The resulting angular diameters and published spectral types are also given in Table 2, in good agreement with Lafrasse et al. (2010), and are all unresolved by the CHARA Array in the *H* band, where the resolution limit for a single star is ≈0.5 mas.

The data were reduced using the standard CHARA reduction pipeline (ten Brummelaar et al. 2005, 2013). The visibilities and closure phases were averaged over each observing block. The calibrated OIFITS data files (Pauls et al. 2005) will be available through the JMMC archive.[2] WR stars have strong emission lines throughout the optical and NIR spectrum (Fig. 1). These emission lines reduce the effective bandpass over which the fringe amplitude is measured causing the true visibility to be smaller than if a fixed bandpass was assumed. We measured the effective bandpass through comparisons of the width of the power spectra of both calibrator stars and the

[2] http://www.jmmc.fr/oidb.htm

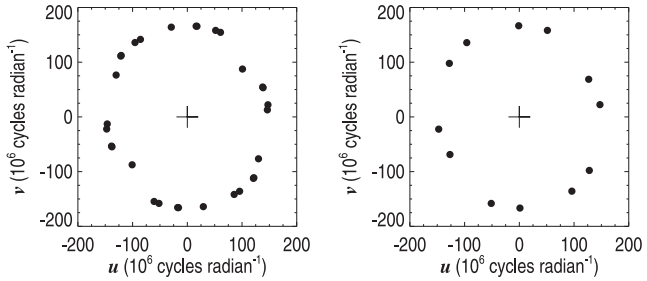

Figure 2. The on-sky (u, v) coverage for WR 137 (left) and WR 138 (right). While fewer observations were made on WR 138, the (u, v) plane is still well covered.

targets, giving a reasonable approximation to the instrumental response. This effect caused the visibilities of WR 137 to change by −15 per cent. The data collected on WR 138 were relatively unaffected by this, and any changes could be accounted for in the measurement errors.

Importantly, the observations are well sampled on the (u, v) plane (Fig. 2), meaning that any fits to the data should provide meaningful measurements of the separation, position angle, and flux ratio for the two stars. We also note that further measurements of these systems were not possible during the observing window as a target of opportunity (Nova Del 2013) became a priority (Schaefer et al. 2014). However, the observations obtained allow for measurements of the binary nature of these stars.

3 RESOLVING THE LONG-PERIOD BINARIES WR 137 AND WR 138

Interferometers measure the fringe contrast or visibility of a source. The complex visibility of a binary system varies periodically (e.g. Boden 2000):

$$V = \frac{V_1 + f V_2 \exp\left[-2\pi i(u\Delta\alpha + v\Delta\delta)\right]}{(1+f)},$$

where $\Delta\alpha$ and $\Delta\delta$ represent the binary separation in right ascension and declination, u and v represent the spatial frequencies of the Array projected on the sky, f represents the flux ratio of the binary, and V_1 and V_2 are the uniform disc visibilities of the primary and secondary components. In our case, we assume the stars are unresolved ($V_1 = V_2 = 1.0$), as a main-sequence O star or the emitting region for $\tau = 1$ optical depth would be smaller than 0.5 mas at the estimated distance of these systems. The real and imaginary parts of the complex visibilities are used to compute the squared visibility amplitude and closure phase to compare with the observations.

Table 3. Binary fits.

Star	Separation (mas)	PA (°)	Date	Phase	f_{WR}	f_O	Reference
WR 137	9.8 ± 0.6	295 ± 1.3	2005 July	0.70	0.56 ± 0.2	0.44 ± 0.2	Rajagopal (2010)
WR 137	4.03 ± 0.02	131.6 ± 0.3	2013 August	0.33	0.59 ± 0.04	0.41 ± 0.04	This work
WR 138	12.37 ± 0.04	305.3 ± 0.2	2013 August	0.31	0.67 ± 0.01	0.33 ± 0.01	This work

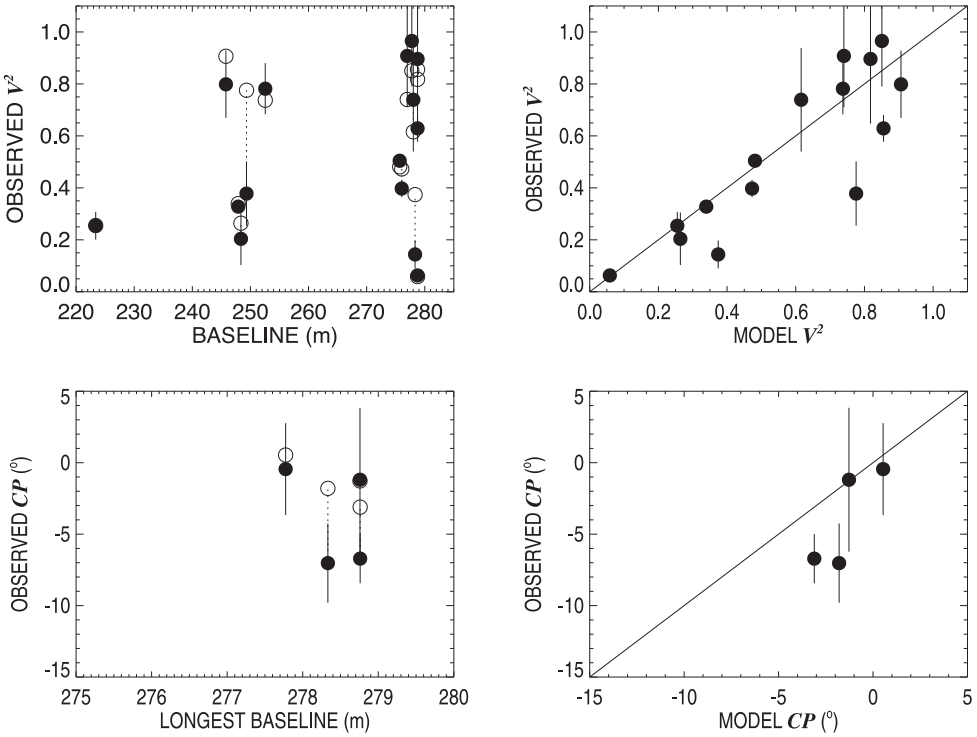

Figure 3. CHARA observations of WR 137. The upper-left plot shows the squared visibilities compared with the baseline, where the filled points represent the measurements and the open circles connected by dotted lines represent the best model (Table 3) for the binary fit. The upper right compares the model and the measurements, with a 1:1 relation overplotted. The lower-left panel shows our four measurements of closure phase (filled points) compared with the longest baseline from the three-telescope configuration, with the model points connected in the same manner as in the upper-left panel. The lower-right panel shows the comparison of the model and the measurements.

We began our analysis using an adaptive grid search procedure where we searched for binary solutions through a large grid of separations in right ascension and declination. At each step in the grid, we optimized the position (ΔRA,ΔDec.) and flux ratio of the binary using the Levenberg–Marquardt least-squares minimization routine MPFIT[3] (Markwardt 2009), and computed the χ^2 statistic for each solution. We performed the adaptive grid search over a range of ±16 mas in ΔRA and ΔDec. using 0.1 mas steps and kept the solution with the lowest χ^2 as the global best-fitting binary model. If the components in the binary are separated by more than the coherence length (∼8 mas for CLIMB measurements on 250–278 m baselines in the *H* band), then they will begin to show two separated fringe packets in the interferometric scans (e.g. Farrington et al. 2010, 2014). We selected a maximum search range of 16 mas, corresponding to twice the coherence length, to represent the separation at which the two fringe packets are completely separated and no longer overlap. Beyond this range, binary components of similar brightnesses would be detected through a visual inspection of the fringes. In order to search out to these wider separations, we added bandwidth smearing to the binary model assuming a rectangular bandpass profile (Kraus et al. 2005).

This method utilized both measurements of visibility and closure phase, which helps to remove the 180° ambiguity in the position angle. The results of these fits are summarized in Table 3, along with the phasing of the binary systems from Annuk (1990, WR 138) and Lefèvre et al. (2005, WR 137), and the fits are shown in the plots of the data in Figs 3 and 4. In general, the model works well for both systems, clearly showing a binary in both cases. Note that in the case of a single star, the visibility function follows a simple Bessel function (e.g. Boyajian et al. 2012), and would also follow a monotonic decrease in the case of a single star with a large wind (e.g. P Cygni; Richardson et al. 2013). As the observations appear as a scatter plot in the upper-left panels of Figs 3 and 4, a resolved binary is the simplest explanation for the systems.

We examined the resulting χ^2 maps from the grid-searching routine, which show an ambiguity in the position of the secondary star reflected across the origin. However, in these mirrored solutions the flux ratio of the binary is also flipped, so in essence, the solutions are identical. The solution with the minimum χ^2 in the maps is reported in Table 3. There are other possible solutions; however, none fall within $\Delta\chi^2 = 3.53$ (the 1σ confidence interval for three fit parameters). These alternative solutions could be further ruled

[3] http://cow.physics.wisc.edu/~craigm/idl/idl.html

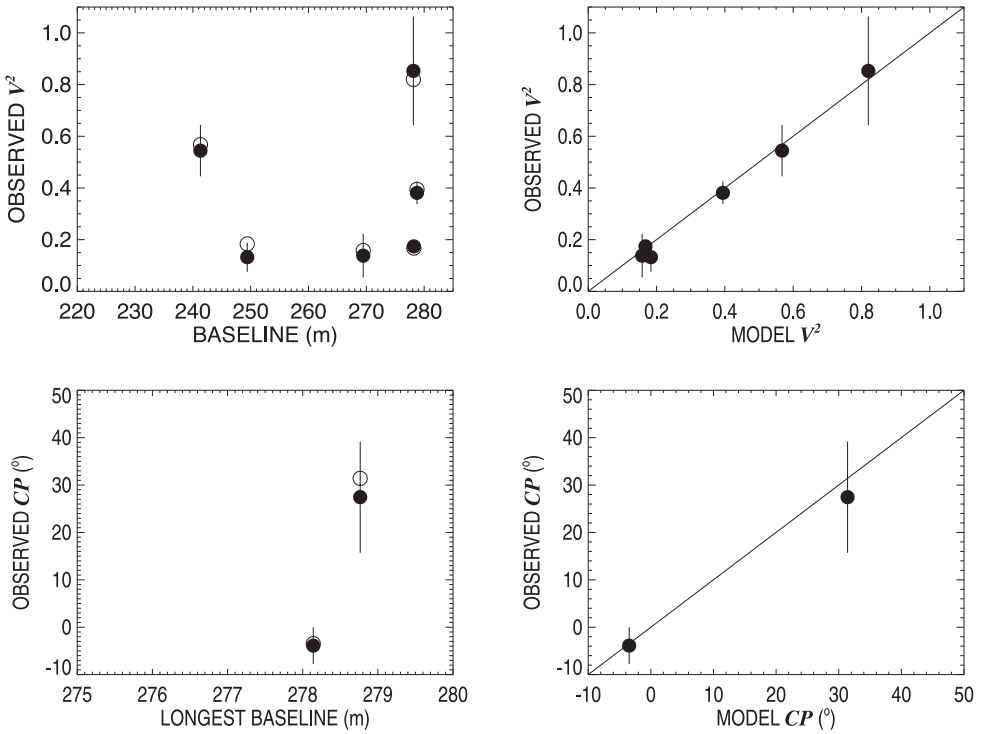

Figure 4. CHARA observations of WR 138, with the same format as Fig. 3.

out by acquiring additional observations in the future and fitting the orbital motion directly to the visibilities and closure phases across multiple epochs.

A visibility near unity would be indicative of a completely unresolved source. If we are partially resolving the WR wind or the O star in these systems, the peak in the visibility curves would be lower than 1. For WR 137 and WR 138, the measured visibilities that are closest to unity are all within the errors from the binary model that assumes that the component stars are unresolved. Moreover, the number of data points is not dense enough to include the angular diameters of the component stars as free parameters in the fit.

4 FLUX RATIOS DERIVED FROM SPECTRAL MODELLING

According to our interferometric measurements for both WR 137 and WR 138, one component slightly dominates over the other in the *H* band. While calibrations of *H*-band magnitudes with spectral types (Martins et al. 2005; Rosslowe & Crowther 2015) imply that the WR component dominates in the *H* band in both systems, the typical magnitude scatter portrayed by WR stars hinders us to conclude this with certainty. To ensure that the relative flux contributions are correctly assigned to the correct components of WR 137 and WR 138, we performed a spectral analysis of both systems using the Potsdam Wolf–Rayet (PoWR;[4] Hamann & Gräefner 2004) non-local thermodynamic equilibrium model atmosphere code, suitable for any hot stars with winds. Comparing synthetic spectra with observations further provides us with the fundamental parameters of the components of each system.

[4] PoWR models of WR stars can be downloaded at http://www.astro.physik.uni-potsdam.de/PoWR.html

A thorough description of the code is beyond the scope of this paper; we only repeat fundamental assumptions here. The prespecified velocity field $v(r)$ takes the form of the β-law (Castor, Abbott & Klein 1975) with $\beta = 1$ and the terminal velocity v_∞ as a free parameter. Clumping is treated via the microclumping approach (Hillier 1984). The clumping factor D is treated as a free parameter for WR models, and is fixed to $D = 10$ in the winds of O-star models (e.g. Feldmeier, Puls & Pauldrach 1997). The depth-dependent microturbulence parameter $\xi(r)$ grows linearly with $v(r)$ from the photospheric value $\xi_{\rm ph}$ to 0.1 v_∞ in the wind, where $\xi_{\rm ph} = 20$ km s^{-1} for O models and $\xi_{\rm ph} = 50$ km s^{-1} for WR models (e.g. Shenar et al. 2015). Macroturbulence is accounted for by convolving the synthetic spectra with appropriate radial-tangential profiles with $v_{\rm mac} = 30$ km s^{-1} (e.g. Gray 1975; Bouret et al. 2012). A more detailed description of the assumptions and methods used in the code is given by Gräfener, Koesterke & Hamann (2002), Hamann & Gräfener (2004), and Sander et al. (2015).

To analyse the systems, we use a multitude of spectra ranging from the UV to the IR. For both objects, all high-resolution, flux-calibrated spectra taken with the *International Ultraviolet Explorer* (*IUE*) in the spectral range 1200–2000 Å were retrieved from the MAST archive. Since the changes with orbital phase in both systems are extremely small, we co-added these spectra to obtain a higher signal-to-noise (S/N $\approx$ 300) for each system. We also retrieved *IUE* spectra covering the range 1900–3100 Å for both systems for a larger coverage of the SED, available in the MAST archive. For WR 137, we utilized a high-resolution, echelle spectrum from the Keck II telescope and the ESI spectrograph. These data were taken near in time to our interferometry, and covered ~4000 Å–1 μm, with a typical S/N across the spectrum of 500 or better. For WR 138, we use complementary, low-resolution ($\Delta\lambda \approx 2$ Å) optical spectra to cover the spectral ranges 3800–4450 Å and 6770–7400 Å, taken between 1991 June 24 and July 1 with the 2.2 m telescope in Calar Alto, Spain (for further details, see Hamann, Koesterke &

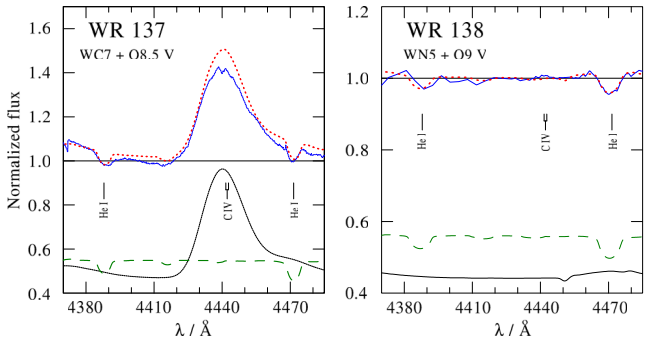

Figure 5. The synthetic composite spectrum (red dotted line) is compared to observations (blue ragged lines) of WR 137 and 138 in the vicinity of the He I λ4471 line. The relative offsets of the WR (black solid line) and O (green dashed line) correspond to the relative light contributions in this spectral range.

Wessolowski 1995) and low-resolution optical spectra obtained at the Observatoire du Mont Mégantic (Québec) near in time to the interferometric observations, spanning ∼4500–6700 Å. We also used the NIR spectra obtained for spectral typing of infrared WR stars by Shara et al. (2012). All spectra were rectified by fitting a low-order polynomial to the apparent continuum.

For both systems, we take *UBV* magnitudes from Neckel, Klare & Sarcander (1980), *R* and *I* magnitude from Monet et al. (2003), and *JHK* magnitudes from Kharchenko (2001). The synthetic spectra are convolved with Gaussians of appropriate widths to mimic the spectral resolution. For WR 137, we also recovered MSX photometry from Egan et al. (2003) and *WISE* photometry from Cutri et al. (2012). Fortuitously, these missions observed WR137 close to the 1997 dust-formation maximum and that expected in 2010 (Williams et al. 2001), respectively. The fluxes are marked A, C, D, and E (MSX) and W1 and W2 (*WISE*) in Fig. 6, where they lie well above the stellar model SED and were not used in the fitting

We represent each binary system as a composite of two models corresponding to their component spectra. As a first step, we calibrate the fundamental parameters of the components against their spectral types. These include the effective temperatures T_* and transformed radii R_t (which are related to the mass-loss rates $\dot{M}$; see Schmutz, Hamann & Wessolowski 1989) for the WR stars, and T_*, $\dot{M}$ and gravities g_* for the O components. We note that T_* and g_* refer to the inner boundary of our models, where the mean Rosseland optical depth $\tau_{\rm Ross} = 20$. For the O companions, the values of these parameters virtually coincide with the photospheric values at $\tau_{\rm Ross} = 2/3$.

With the parameters fixed, the light ratio can be derived by examining a multitude of features in the available spectra, primarily in the UV and optical. An example is shown in Fig. 5, where the best-fitting models for both systems are compared to optical observations in the vicinity of the He I λ4471 line. This line maintains an almost identical equivalent width in the temperature domain 30–35 kK, which is the relevant temperature domain for both O companions concerned here. Its strength is therefore directly related to the dilution factor, i.e. the light ratio in the visual. In contrast, the He I λ4388 line, also shown in Fig. 5, is sensitive to T_* and g_*. The derived light ratios are consistent with a multitude of features in the available spectra. We further confirmed our results by comparing with equivalent width calibrations for single O stars (e.g. Conti & Alschuler 1971).

The stellar parameters are then further refined until no significant improvement can be achieved. Wind parameters are derived based on the strengths and shapes of emission lines. For the O stars, v_∞ could be constrained from the C IV and Si IV resonance lines. Their mass-loss rates are very roughly constrained based on the existence of P Cygni or emission features clearly associated with the O components or lack thereof. The projected rotational velocity $v \sin i$ is derived primarily from He I and He II lines (see e.g. Fig. 5). The components' luminosities L and the reddening $E(B-V)$ are derived by comparing the composite synthetic spectrum to the SED of each system. We assume the reddening law given by Seaton (1979) with $R_V = 3.1$. We adopt distances from Rosslowe & Crowther (2015), which result in consistent luminosities for both parameters.

The SEDs and spectra along with the best-fitting models are shown in Figs 6 and 7. The derived parameters are listed in Table 4. Uncertainties are estimated based on the sensitivity of the fit quality to changes in the corresponding parameter. The table also gives stellar radii R_* (calculated via the Stefan–Boltzmann law), *V*- and *H*-band magnitudes, and extinctions A_V. Our results turn out to be very consistent with what is expected for stars of the given spectral types. The derived light ratios indeed imply that the WR component is the dominant source in the *H* band in both systems. For WR 137, the WR component contributes (59 ± 4) per cent of the *H*-band flux as derived by the interferometry, and is seen to contribute a fractional flux of 0.59 in the PoWR model. Similarly, for WR 138, we measured the WR component to contribute (67 ± 1) per cent of the *H*-band flux, with the PoWR results showing the fraction to be 0.66. These measurements show the strong agreement in the two methods, and strengthen the results of both investigations.

5 DISCUSSION

The interferometric measurements of WR 138 represent the first time a WN star has been resolved in a spectroscopic binary. We note that the fundamental parameters derived through our spectroscopic modelling of the binary system agree with the expectations for a late O dwarf (Martins et al. 2005; Martins & Plez 2006) as the companion. The absorption lines in the system are very broad and shallow (see Figs 5 and 7), and have caused some controversy in the literature. The star was first called a binary based upon the absorption lines of hydrogen and neutral helium in the blue by Hiltner (1945). Massey (1980) studied a time series of moderate-resolution photographic spectra to find that the semi-amplitude of any binary would likely be $\lesssim$30 km s^{-1} for periods less than 6 months, for which his RV study is most sensitive.

Lamontagne et al. (1982) examined a longer time series of spectra of WR 138, including the measurements of Massey (1980) and Bracher (1966). They found a long-period orbit, with a period of ∼1700 d, and attributed short-term variability of the WR emission lines as arising from a short-period, 2.3 d, orbit with a neutron star. The short-period orbit was not confirmed when Annuk (1990) later examined the system and concluded that the system was a spectroscopic binary, with a period of ∼1500 d. The O star is fairly exotic compared to most O dwarfs, as the measured value of $v \sin i$ is roughly 500 km s^{-1} (Massey 1980; Annuk 1990; Hamann, Gräefener & Liermann 2006), while our spectral modelling indicates a lower value of ∼350 km s^{-1}. This is incredibly high in comparison to the population of O stars both in the Galaxy (Howarth et al. 1997) and even in the massive, star-forming region of 30 Dor (Ramírez-Agudelo et al. 2013), where the measured $v \sin i$ would place the companion in the top 5–10 per cent of the population.

The period derived by Annuk (1990) and Palate et al. (2013) is quite long (4.2 yr), and should be longer than typical orbits associated with binary interactions (e.g. Sana et al. 2012). However, the period limit for a zero-age main-sequence O star to experience

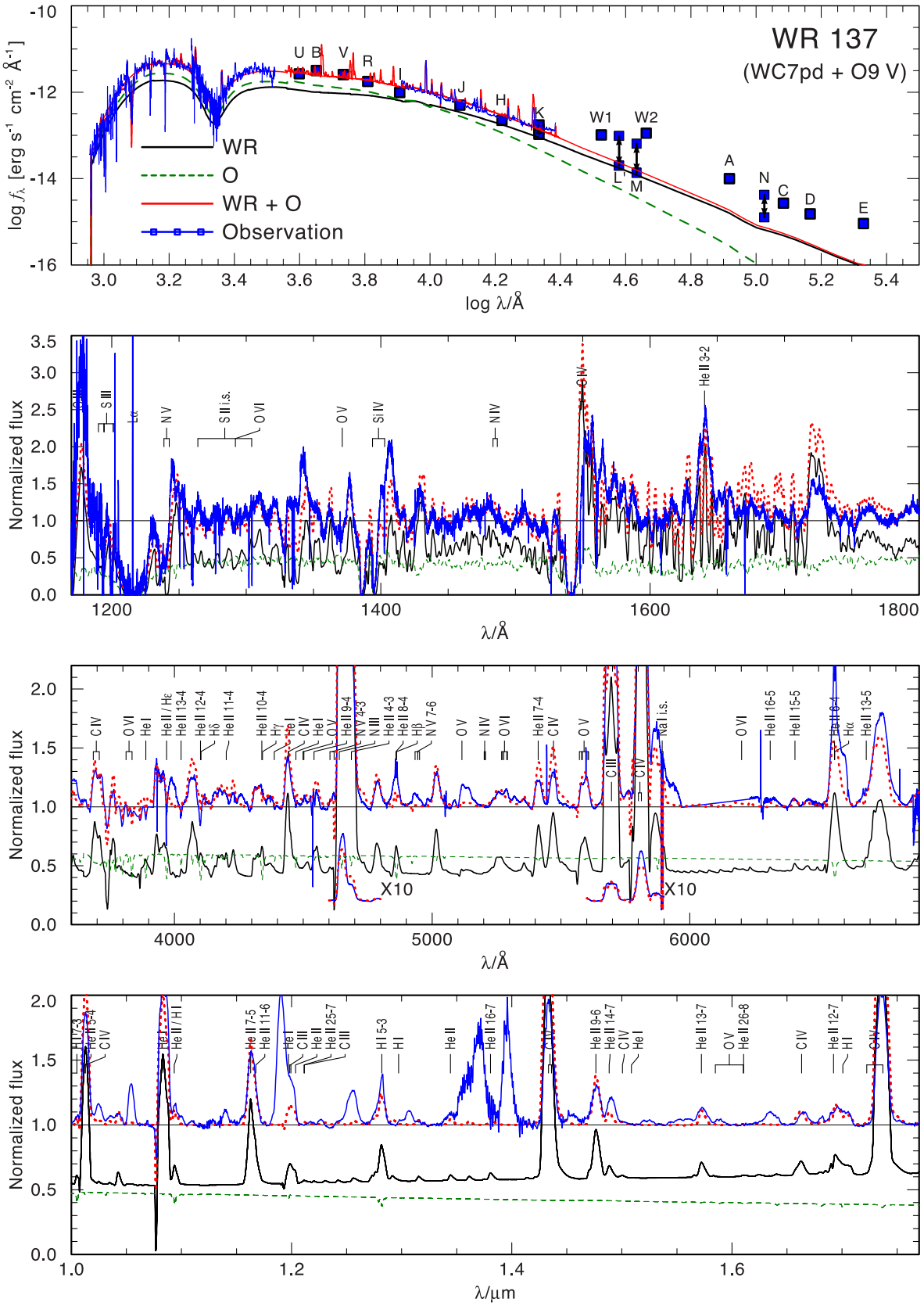

Figure 6. The best-fitting synthetic SED (upper panel) and normalized spectrum (lower panels) compared to observations of WR 137 (blue lines and squares). The composite model is the superposition of the WR (black solid line) and O (green dashed line) models. The relative offsets of the model continua shown in the lower panels depict the relative light contribution in each spectral range. The few arrows shown in the upper panel illustrate the IR excess variability in the system from Williams et al. (2001). Note that the CHARA observations were collected in the *H* band (log λ ≈ 4.2).

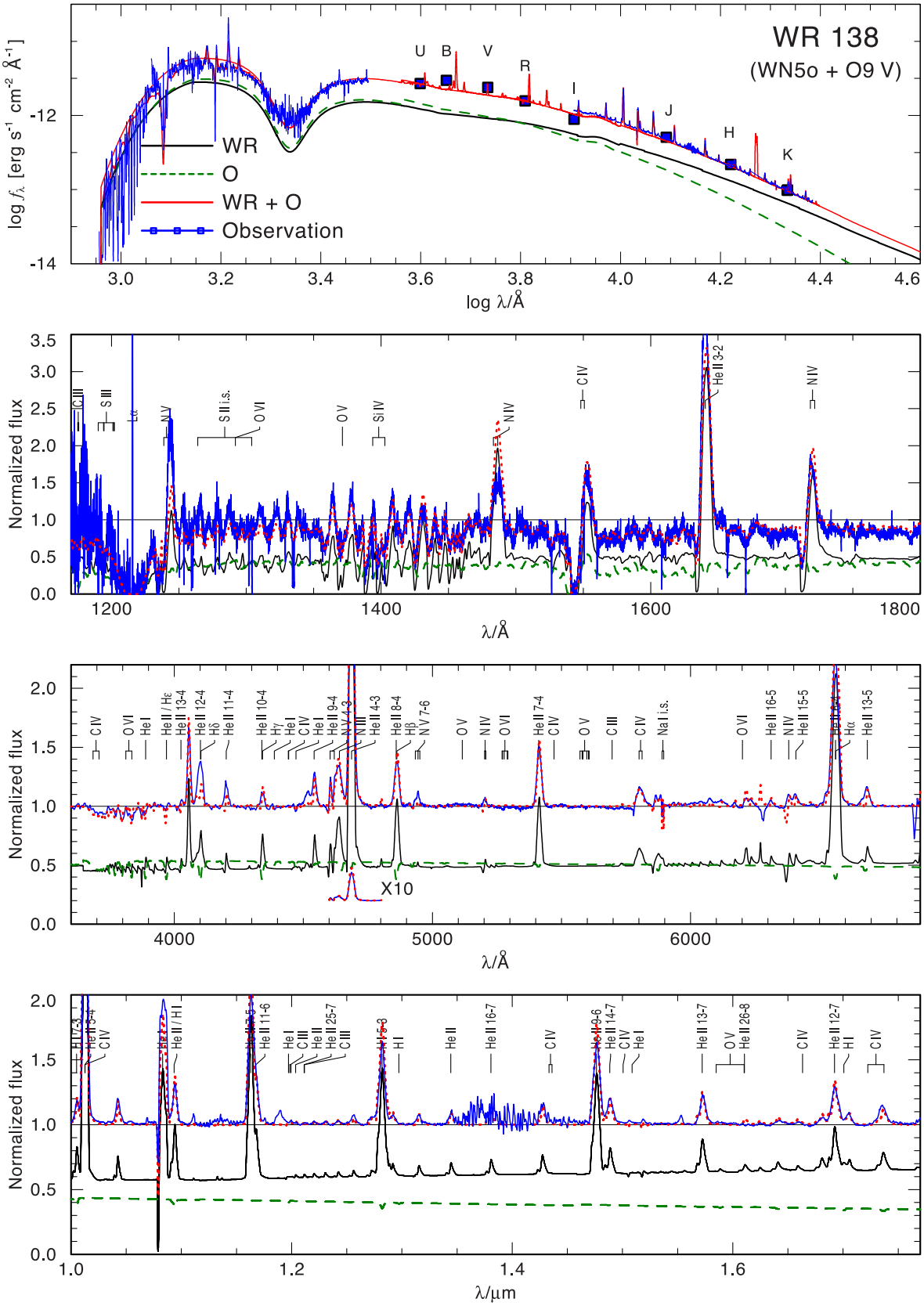

Figure 7. As Fig. 6, but for WR 138. Note that the CHARA observations were collected in the *H* band (log λ ≈ 4.2).

Table 4. Inferred stellar parameters for WR 137 and 138.

	WR 137		WR 138	
Component	WR	O	WR	O
Distance d (pc)	1300		1380	
Spectral type	WC7pd	O9 V	WN5o	O9 V
T_* (kK)	60^{+5}_{-5}	32^{+2}_{-2}	56^{+5}_{-5}	31^{+2}_{-2}
$\log g_*$ (cm s^{-2})	–	$4.0^{+0.3}_{-0.3}$	–	$4.0^{+0.3}_{-0.3}$
$\log L$ ($L_\odot$)	$5.22^{+0.05}_{-0.05}$	$4.75^{+0.05}_{-0.05}$	$5.35^{+0.05}_{-0.05}$	$4.82^{+0.05}_{-0.05}$
$\log R_t$ ($R_\odot$)	$0.7^{+0.05}_{-0.05}$	–	$0.9^{+0.05}_{-0.05}$	–
v_∞ (km s^{-1})	1700^{+100}_{-100}	1800^{+100}_{-100}	1200^{+100}_{-100}	2000^{+200}_{-200}
R_* ($R_\odot$)	3.8^{+1}_{-1}	7.7^{+1}_{-1}	4.8^{+2}_{-2}	8.9^{+2}_{-2}
D	4	10	10	10
$\log \dot{M}$	$-4.65^{+0.2}_{-0.2}$	$-7.1^{+1.0}_{-0.3}$	$-5.15^{+0.2}_{-0.2}$	$-7.7^{+0.5}_{-1.5}$
$v \sin i$ (km s^{-1})	–	220^{+20}_{-20}	–	350^{+30}_{-30}
M_V (mag)	$-4.18^{+0.2}_{-0.2}$	$-4.34^{+0.2}_{-0.2}$	$-4.40^{+0.2}_{-0.2}$	$-4.53^{+0.2}_{-0.2}$
M_H (mag)	$-4.07^{+0.2}_{-0.2}$	$-3.41^{+0.2}_{-0.2}$	$-4.28^{+0.3}_{-0.3}$	$-3.60^{+0.3}_{-0.3}$
$E(B-V)$ (mag)	$0.74^{+0.02}_{-0.02}$		$0.67^{+0.02}_{-0.02}$	
A_V (mag)	$2.29^{+0.06}_{-0.06}$		$2.08^{+0.06}_{-0.06}$	

spin-up from a companion from the results of Sana et al. (2012) is actually similar to the orbital period of WR 138. Therefore, the extreme rapid rotation of this companion may actually be the remnant of a past interaction where the current WR star lost mass via Roche lobe overflow which then deposited angular momentum and mass on to the O star. If the semi-major axis is conserved in this process, then if the original system were $30 + 20\,M_\odot$ stars that interacted to become $15 + 25\,M_\odot$ stars through a combination of mass-loss and accretion, the period would have originally been shorter (<1400 d) and near the adopted upper limits for an interacting binary as defined by Sana et al. (2012).

These interferometric observations of WR 137 represent the second reported binary measurements of this star. Rajagopal (2010) found a binary flux ratio equal to our measurements. However, the projected separations between our measurements and those of Rajagopal (2010) differ by about a factor of 2, and they differ by ∼180°, but were taken at opposite quadratures. Two measurements of separation and position angle from two different instruments are not enough to warrant an attempt of a visual orbit. Further, we note that we are unsure if Rajagopal (2010) accounted for the contamination of emission lines in the interferometry, which can alter the measured separation and position angle. However, it seems that the eventual orbital solution will favour a system with a nearly edge-on geometry.

A directly edge-on system will have masses that are perhaps lower than expected in the WR 137 system, but there are supporting reasons to trust the inclination to be closer to edge-on. Marchenko et al. (1999) imaged the system in the H and K bands with the *Hubble Space Telescope* (*HST*) and the NICMOS camera. These images were taken during and after a periastron passage when dust is formed. These images revealed structures in the K band, but not in the H band, that were thought to have emerged from the wind–wind collision region. It is interesting that the position angle of the structure imaged by *HST* is ≈110°. If the positions measured by the IOTA and CHARA interferometers are indeed pointing towards an edge-on orbit, then the dust formation may occur near the orbital plane. Further observations can elucidate the details of the orbit and the formation region of the dust. We also note that the opening angle of the shock cone is ≈20° according to the approximations given by Gayley (2009) and our spectral modelling, so the small opening angle in the *HST*/NICMOS imaging is consistent with this explanation.

Clearly, the next step in these systems is twofold. We need to resolve the orbits at multiple epochs in order to measure the visible orbit of the systems. This will lead to constraints on the inclinations of the system and the orbit. Contemporaneous to this, we need to re-determine the double-lined spectroscopic orbits of these systems as both orbits are poorly constrained for the O star components. The O star in the WR 138 system is extremely difficult to measure due to its large value for $v \sin i$, so high-resolution spectroscopy with high S/N is needed. The resolution and interferometric follow-up of WR 137 and WR 138 will double the number of the masses measured for WR stars in longer period orbits, with WR 138 being the first WN star with a visual orbit. Future interferometry of WR 137 would benefit from measurements made in both the H and K bands near in time so that the binary parameters can first be resolved in the H band. These derived parameters can then be used to pinpoint the exact place where the dust formation happens in the close environs of the system. Such observations can be used to further understand the K-band *HST* imaging of the system that was reported by Marchenko et al. (1999). WR 137 provides an exciting example of a WC+O system where we can determine empirically the location of the dust formation through long-baseline infrared interferometry and then compare the close environs of the system's dust production to the larger scale imaging reported by Marchenko et al. (1999).

ACKNOWLEDGEMENTS

We wish to thank Michael Shara, Jacqueline Faherty, and Graham Kanarek for allowing us to use their NIR spectra of these two stars. We thank the CHARA staff for supporting these observations and the Mount Wilson Institute for its continued support of the CHARA Array. This material is based upon work supported by the National Science Foundation under Grants AST-1211929 and AST-1411654. Some of the spectroscopic data were obtained at the W. M. Keck Observatory on the summit of Mauna Kea. We wish to recognize and acknowledge the very significant cultural role and reverence that the summit of Mauna Kea has always had within the indigenous Hawaiian community. We are most fortunate to have the opportunity to conduct observations from this mountain. The *IUE* data presented in this paper were obtained from the Mikulski Archive for Space Telescopes (MAST). STScI is operated by the Association of Universities for Research in Astronomy, Inc., under NASA contract NAS5-26555. Support for MAST for non-*HST* data is provided by the NASA Office of Space Science via grant NNX09AF08G and by other grants and contracts.

NDR acknowledges postdoctoral support by the University of Toledo and by the Helen Luedtke Brooks Endowed Professorship, and is thankful for his former CRAQ (Québec) fellowship which supported him at the beginning of this research. TS is grateful for financial support from the Leibniz Graduate School for Quantitative Spectroscopy in Astrophysics, a joint project of the Leibniz Institute for Astrophysics Potsdam (AIP) and the institute of Physics and Astronomy of the University of Potsdam. AFJM and NSL are grateful for financial aid from NSERC (Canada) and FQRNT (Quebec). PMW is grateful to the Institute for Astronomy for continued hospitality and access to the facilities of the Royal Observatory Edinburgh.

REFERENCES

Aldoretta E. J. et al., 2015, AJ, 149, 26
Annuk K., 1990, Acta Astron., 40, 267
Barbier M., 1963, Publ. Obs. Haute-Provence, 6, 36
Boden A. F., 2000, in Lawson P. R., ed., Principles of Long Baseline Stellar Interferometry. Jet Propulsion Laboratory, Pasadena, CA, p. 9
Bouret J. C., Hillier D. J., Lanz T., Fullerton A. W., 2012, A&A, 544, 67
Boyajian T. S. et al., 2012, ApJ, 746, 101
Boyajian T. S., van Belle G., von Braun K., 2014, AJ, 147, 47
Bracher K., 1966, PhD thesis, Indiana University
Castor J. I., Abbott D. C., Klein R. I., 1975, ApJ, 195, 157
Conti P. S., Alschuler W. R., 1971, ApJ, 170, 325
Cutri R. M. et al., 2012, VizieR Online Data Catalogs: II/311
De Marco O., Schmutz W., 1999, A&A, 345, 163
De Marco O., Schmutz W., Crowther P. A., Hillier D. J., Dessart L., de Koter A., Schweickhardt J., 2000, A&A, 358, 187
Egan M. P. et al., 2003, VizieR Online Data Catalogs: V/114
Fahed R. et al., 2011, MNRAS, 418, 2
Farrington C. D. et al., 2010, AJ, 139, 2308
Farrington C. D. et al., 2014, AJ, 148, 48
Feldmeier A., Puls J., Pauldrach A. W. A., 1997, A&A, 322, 878
Gayley K. G., 2009, ApJ, 703, 89
Gräfener G., Koesterke L., Hamann W.-R., 2002, A&A, 387, 244
Gray D. F., 1975, ApJ, 202, 148
Hamann W.-R., Gräefener G., 2004, A&A, 427, 697
Hamann W.-R., Koesterke L., Wessolowski U., 1995, A&AS, 113, 459
Hamann W.-R., Gräefener G., Liermann A., 2006, A&A, 457, 1015
Hanbury Brown R., Davis J., Herbison-Evans D., Allen L. R., 1970, MNRAS, 148, 103
Hillier D. J., 1984, ApJ, 280, 744
Hiltner W. A., 1945, ApJ, 101, 356
Honeycutt R. K., McCuskey S. W., 1966, PASP, 78, 289
Howarth I. D., Siebert K. W., Hussain G. A. J., Prinja R. K., 1997, MNRAS, 284, 265
Kharchenko N. V., 2001, Kinematika Fiz. Nebesnykh Tel., 17, 409
Kraus S. et al., 2005, AJ, 130, 246
Lafrasse S., Mella G., Bonneau D., Duvert G., Delfosse X., Chesneau O., Chelli A., 2010, Proc. SPIE, 7734, 140
Lamontagne R., Koenigsberger G., Seggewiss W., Moffat A. F. J., 1982, AJ, 253, 230
Lefèvre L. et al., 2005, MNRAS, 360, 141
Ljunggren B., Oja T., 1961, Uppsala Astron. Obs. Ann., 4, 1
Marchenko S. V., Moffat A. F. J., Grosdidier Y., 1999, ApJ, 522, 433
Markwardt C. B., 2009, in Bohlender D. A., Durand D., Dowler P., eds, ASP Conf. Ser. Vol. 411, Astronomical Data Analysis Software and Systems XVIII. Astron. Soc. Pac., San Francisco, p. 251
Martins F., Plez B., 2006, A&A, 457, 637
Martins F., Schaerer D., Hillier D. J., 2005, A&A, 436, 1049
Massey P., 1980, ApJ, 236, 526
Millour F. et al., 2007, A&A, 464, 107
Monet D. G. et al., 2003, AJ, 125, 984
Monnier J. D. et al., 2004, ApJ, 602, L57
Monnier J. D. et al., 2011, ApJ, 742, L1
Neckel T., Klare G., Sarcander M., 1980, Bull. Inf. Cent. Donnees Stellaires, 19, 61
North J. R., Tuthill P. G., Tango W. J., Davis J., 2007, MNRAS, 377, 415
Nugis T., Lamers H. J. G. L. M., 2000, A&A, 360, 227
Palate M., Rauw G., De Becker M., Nazé Y., Eenens P., 2013, A&A, 560, 27
Pauls T. A., Young J. S., Cotton W. D., Monnier J. D., 2005, PASP, 117, 1255
Rajagopal J., 2010, Rev. Mex. Astron. Astrofis. Ser. Conf., 38, 54
Ramírez-Agudelo O. H. et al., 2013, A&A, 560, 29
Richardson N. D. et al., 2013, ApJ, 769, 118
Rosslowe C. K., Crowther P. A., 2015, MNRAS, 447, 2322
Sana H. et al., 2012, Science, 337, 444
Sana H. et al., 2014, ApJS, 215, 15
Sander A. et al., 2015, A&A, 577, 13
Schaefer G. H. et al., 2014, Nature, 515, 234
Schmutz W., Hamann W.-R., Wessolowski U., 1989, A&A, 210, 236
Schmutz W. et al., 1997, A&A, 328, 219
Seaton M. J., 1979, MNRAS, 187, 73
Shara M. M., Faherty J. K., Zurek D., Moffat A. F. J., Gerke J., Doyon R., Artigau E., Drissen L., 2012, AJ, 143, 149
Shenar T. et al., 2015, ApJ, 809, 135
Smith N., Owocki S., 2006, ApJ, 645, L45
Smith L. F., Shara M. M., Moffat A. F. J., 1996, MNRAS, 281, 163
ten Brummelaar T. A. et al., 2005, ApJ, 628, 453
ten Brummelaar T. A. et al., 2013, J. Astron. Instrum., 2, 1340004
Tuthill P., Monnier J. D., Lawrance N., Danchi W. C., Owocki S. P., Gayley K. G., 2008, ApJ, 675, 698
Williams P. M., Longmore A. J., van der Hucht K. A., Talevera A., Wamsteker W. M., Abbott D. C., Telesco C. M., 1985, MNRAS, 215, 23
Williams P. M. et al., 2001, MNRAS, 324, 156

This paper has been typeset from a TEX/LATEX file prepared by the author.